

FRAGMENT OF AN AEGIS OF NEÏTH 1886.305.0096 – LEADED BRONZE

Artefact name	Fragment of an Aegis of Neïth 1886.305.0096
Authors	Line. Pedersen (HE-Arc, Neuchâtel, Neuchâtel, Switzerland)
Url	/artefacts/315/

✧ The object



Fig. 1: Fragment of an Aegis of Neïth, consisting of a copper alloy. From left to right: front, side view and back respectively,

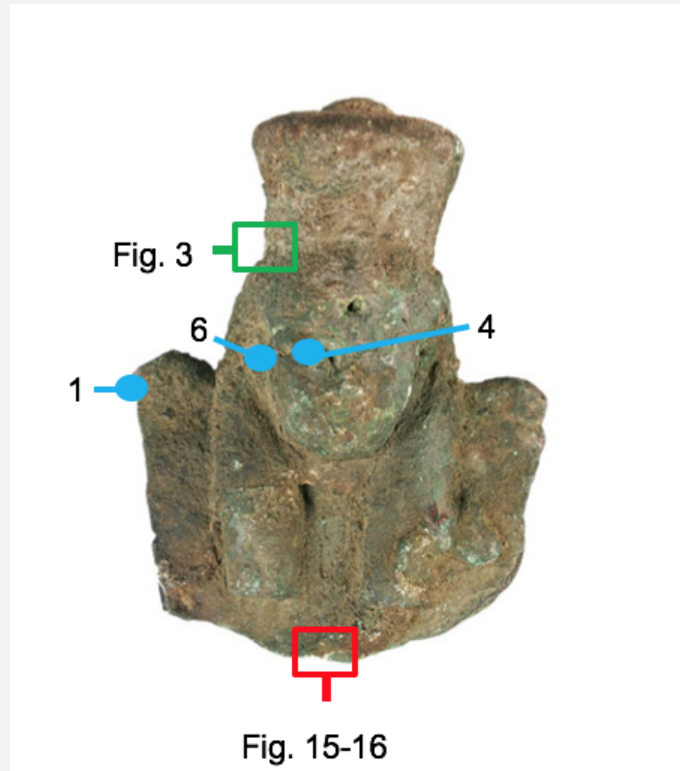
Credit He-Arc CR, L. Pedersen

✧ Description and visual observation

Description of the artefact	<p>Fragment of an aegis, consisting of a cast copper alloy and surmounted by the head of Neith, the Egyptian goddess of war. Traces of leaf gilding is still present in certain areas. The lower part of the collar and the upper part of the crown are broken. The surface is covered with a thick and hard, green-brown corrosion crust. A cross-section was studied on the lower edge that was broken after excavation.</p> <p>Dimensions: L = 96mm; W = 72mm; T = 40mm; WT = 216g.</p>
Type of artefact	Aegis
Origin	ancient Egypt
Recovering date	Purchased at the end of the 19th, probably from the art market. Date of excavation unknown.
Chronology category	None
chronology tpq	<input type="text"/> ---- ▼
chronology taq	<input type="text"/> ---- ▼
Chronology comment	Unknown
Burial conditions / environment	Unknown

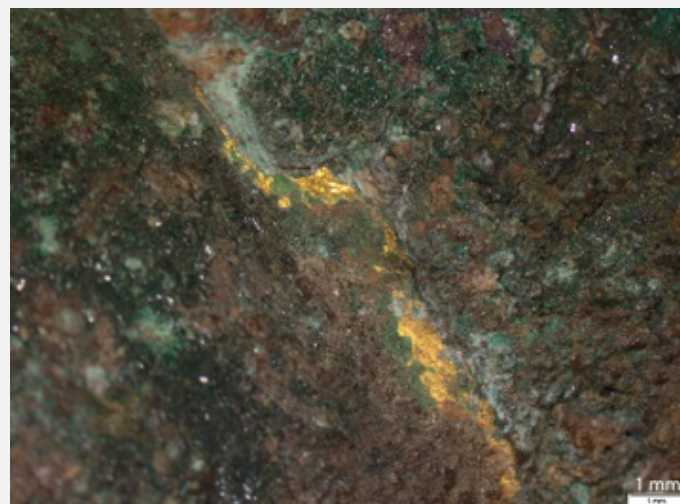
Artefact location	Bernisches Historisches Museum (BHM), Bern, Bern
Owner	Bernisches Historisches Museum (BHM), Bern, Bern
Inv. number	1886.305.0096
Recorded conservation data	Unknown

Study area(s)



Credit He-Arc CR, L.Pedersen.

Fig. 2: Front face: location of XRF measurements (blue spots), powder sample (red square) and gilding remains on the surface (green square),



Credit He-Arc CR, L.Pedersen.

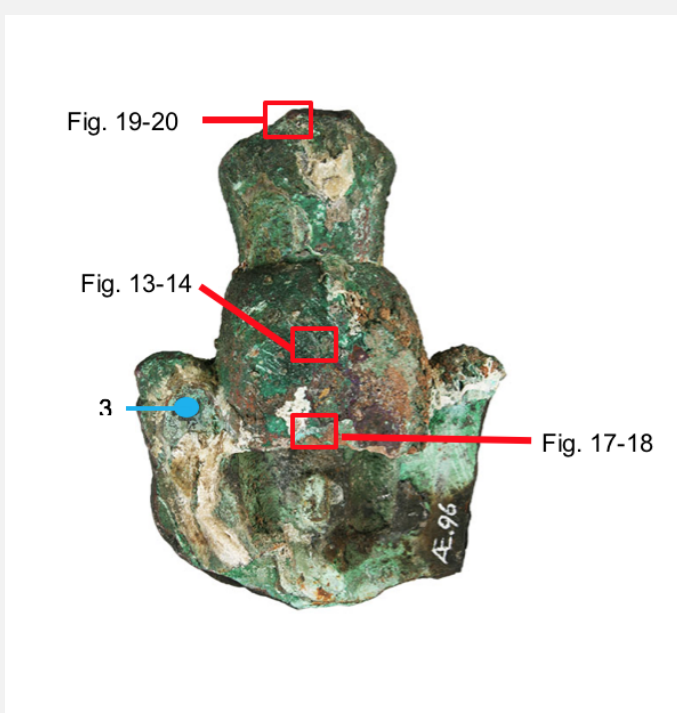
Fig. 3: Remains of foil-gilding on the corroded surface,

Fig. 4: Side view: location of XRF measurements (blue spots),



Credit He-Arc CR, L.Pedersen.

Fig. 5: Back face: location of XRF measurement (blue spot) and powder samples (red squares),

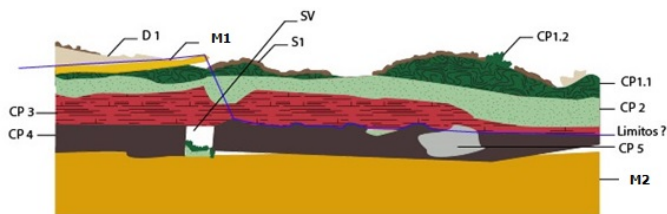


Credit He-Arc CR, L.Pedersen.

✧ Binocular observation and representation of the corrosion structure

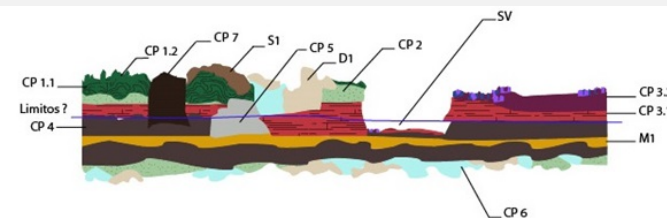
The schematic representation below gives an overview of the corrosion layers encountered on the object from visual macroscopic inspection.

Fig. 6: Preliminary stratigraphy 1, corresponding to the front face of the artefact. S = soil, D = deposit, M = metal, CP = corrosion products, SV = structural void,



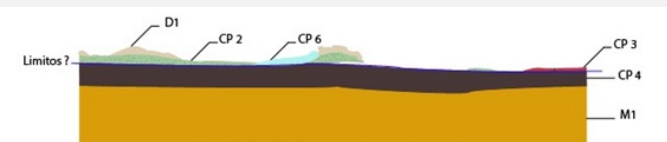
Captions	Colour, aspect, hardness and cohesion
S1	Brown, matte, can be scratched with scalpel blade but remains cohesive.
D1	White deposit: shiny, powdery when shaved with scalpel.
M1	Thin gold leaf trapped in corrosion products, brittle, yellow and not adherent.
CP1.1	Dark green corrosion layer, lumpy and matte, thick, hardly scratched by a scalpel blade, cohesive and compact.
CP1.2	Minor stratum of CP1.1. Dark green crystals appearing on the surface of the artefact. Easily scratched under the action a scalpel blade.
CP2	Light green corrosion layer, matte, thick in some places, powdery under the action of a scalpel blade. In some areas it is located directly on CP4.
CP3	Red corrosion layer, lumpy and matte, thick, sometimes hard and sometimes powdery under the action of a scalpel blade.
Limitos	Interface of the limit of the original surface. Shiny, straight and black with manufacturing traces.
CP4	Dark grey with red or green reflection. Shiny, hard, straight, dense and with traces of engraving and possible inlays.
CP5	Isolated white corrosion products: waxy and very soft.
SV	Void in CP4 resulting in loss of the limitos.
M2	Yellow stratum with metallic sheen, dense and hardly scratched by scalpel blade.

Credit He-Arc CR, L.Pedersen.



Captions	Colour, aspect, hardness and cohesion
S1	Brown, matte, can be scratched with scalpel blade but remains cohesive.
D1	White shiny deposit, powdery when shaved with scalpel.
CP1.1	Dark green corrosion layer, lumpy and matte, thick, hardly scratched by a scalpel blade, cohesive and compact.
CP1.2	Minor stratum of CP1.1. Dark green crystals appearing on the surface of the artefact. Easily scratched by a scalpel blade.
CP2	Light green corrosion layer, matte and thick in some places, powdery under the action of a scalpel blade. Sometimes located directly on CP4.
CP3.1	Red corrosion layer, lumpy and matte, thick, sometimes hard and sometimes powdery under the action of a scalpel blade.
CP3.2	Minor stratum of CP3.1. Purple with blue-purple crystals, hard and cohesive.
Limitos	Interface of the limit of the original surface. Shiny, straight, black, manufacturing traces.
CP4	Dark grey with red or green reflection. Shiny, hard, straight, dense and with traces of engraving and possible inlays.
CP5	Isolated white stratum: waxy and very soft.
CP6	Light blue stratum, chalky. Isolated on the exterior surface and extends on the interior surface.
CP7	Isolated black stratum, very hard, straight and shiny.
SV:	Void in CP4, resulting in loss of the limitos. Presence of CP1.2 crystals inside the void.
Structural Void	
M1	Yellow stratum with metallic sheen, dense and hardly scratched by scalpel blade.

Credit He-Arc CR, L.Pedersen.



Captions	Colour, aspect, hardness and cohesion
D1	White shiny deposit, powdery when shaved with scalpel.
CP2	Light green corrosion layer, matte and thick in some places, powdery under the action of a scalpel blade. Sometimes located directly on CP4.
CP3	Red corrosion layer, lumpy and matte, thick, sometimes hard and sometimes powdery under the action of a scalpel blade.
Limitos	Interface of the limit of the original surface. Shiny, straight, black and with manufacturing traces.
CP4	Dark grey with red or green reflection. Shiny, hard, straight, dense and with traces of engraving and possible inlays.
CP6	Light blue stratum, chalky. Isolated on the exterior surface and extends on the interior surface.
M1	Yellow stratum with metallic sheen, dense and hardly scratched by scalpel blade.

Fig. 7: Preliminary stratigraphy 2, corresponding to the back face and interior (below part). S = soil, D = deposit, M = metal, CP = corrosion products, SV = structural void,

Fig. 8: Preliminary stratigraphy 3, corresponding to the area of the back with a well-preserved limit of original surface. S = soil, D = deposit, M = metal, CP = corrosion products,

⌵ MiCorr stratigraphy(ies) – Bi

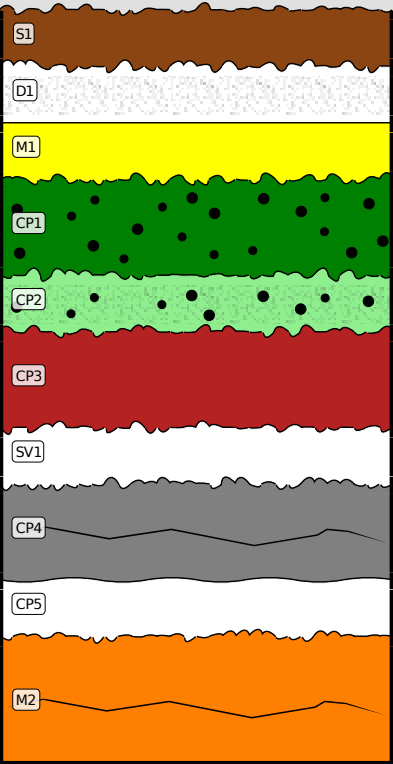


Fig.9: Schematic representation combining stratigraphies 1 and 2, Credit He-Arc CR, L.Pedersen.

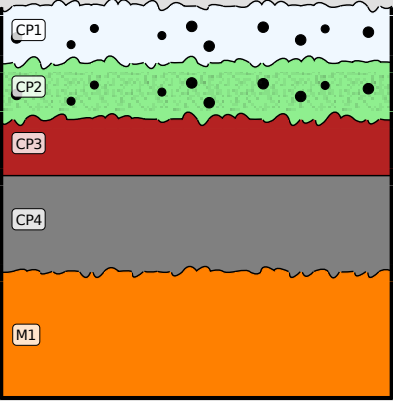


Fig.10: Schematic representation of stratigraphy 3, Credit He-Arc CR, L. Pedersen.

⌵ Sample(s)

Description of sample	Only samples of corrosion products were taken. For sampling locations, see Figs. 2-5.
Alloy	Leaded Bronze
Technology	As-cast, engraving, (glass?) inlay, gilding with gold foil.
Lab number of sample	None
Sample location	HE-Arc CR, Neuchâtel, Neuchâtel

Responsible institution	HE-Arc CR, Neuchâtel, Neuchâtel
Date and aim of sampling	April 11th 2017, chemical and molecular analyses

≡ Analyses and results

X-Ray Tomography of the entire object with MICRODETECT system: 1600 projections of 2000x2000pixels, V = 280kV, I = 100uA, filter of copper (0.5mm) and aluminium (2mm), integration time per projection: 3s/image x 2 images, total time acquisition: 1600 x 6s and distance source-detector: 1225mm.

X-Ray Fluorescence (XRF) on the object under the corrosion crust and on cross-section with portable X-ray fluorescence spectrometer (NITON XL3t 950 Air GOLDD+ analyser, ThermoFischer®).

X-Ray diffraction (XRD) on corrosion product. Data collected was performed using Mo-K α radiation ($\lambda = 0.71073\text{\AA}$, beam diameter 0.5mm) and XRD patterns measured on a Stoe Mark II-Imaging Plate Diffractometer System equipped with a graphite-monochromator. Two-dimensional diffraction images (10min per exposure) were obtained at an image plate distance of 200mm with a continued sample rotation. Resolution of Dmax 24.00 and Dmin 1.04 \AA and intensity integration performed over the entire image (360°).

≡ Non invasive analysis

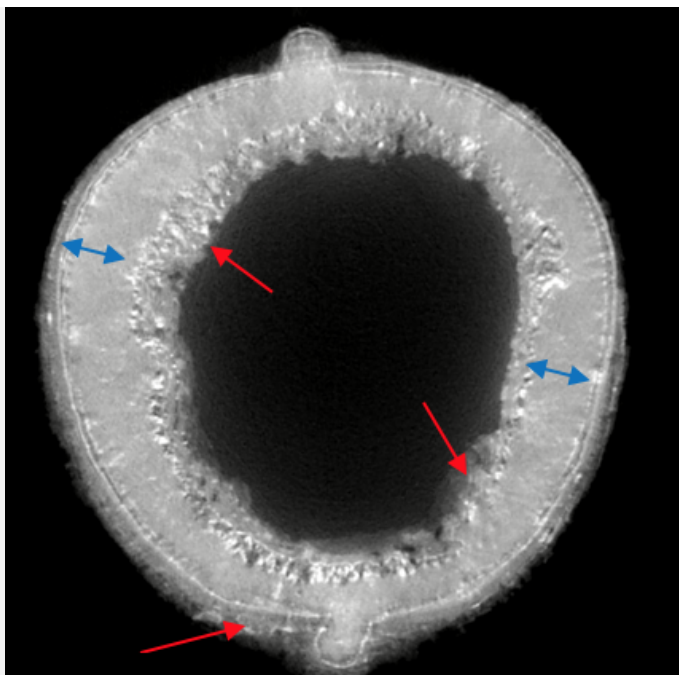
≡ Metal

The metal (M2 in Fig.9 and M1 in Fig. 10) was analysed on the broken edge of the bottom of the artefact where despite a highly corroded surface, the metal seems to be well preserved. A tomography confirmed this hypothesis (see Figs. 11-12).The XRF analyses revealed that the metal is a leaded bronze with remains of gold leaf on the surface (table 1, Au was detected in the measurement spots 4,5 and 6) (Scott et Swartz, 2002; Gouda et al., 2012; Mohammed et Darweesh, 2012).

Areas/ elements (mass%)	Cu	Pb	Sn	Sb	Ag	Zn	Ni	Pd	Au	Si	Al	Fe	S	Ti	P	Cd
1	68.9	9.5	0.2	0.06	<	<	0.04	<	<	13.4	3.7	1.4	2.2	0.2	0.3	<
2	78.1	12.3	2.4	0.3	0.2	<	0.1	<	<	2.8	1.8	1.9	<	0.1	<	<
3	83.3	11.6	1.4	0.2	<	<	0.04	<	<	1.4	1.3	0.5	<	0.05	<	<
4	80.6	11.4	0.5	<	0.2	0.08	0.1	0.1	0.9	<	<	2.1	<	0.5	<	0.1
5	76.5	11.3	0.5	<	0.4	0.1	0.1	0.2	6.6	<	<	2.8	<	0.7	<	0.2
6	89.8	5.6	0.2	<	0.2	0.1	0.4	0.1	1.8	<	<	1.1	<	0.2	<	0.08

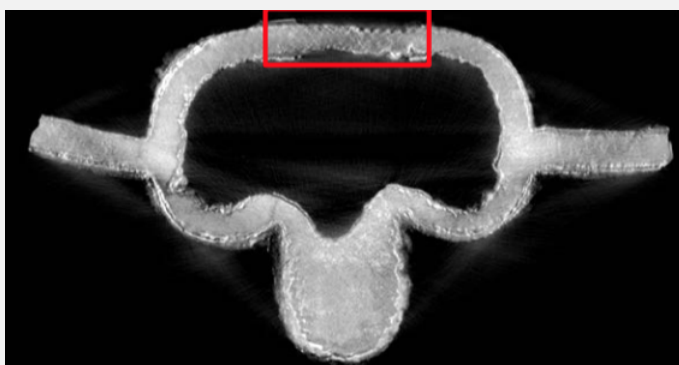
Table 1: Chemical composition of the artefact in the areas located on figures 2, 4 and 5. Method of analysis: portable XRF, acquisition time 60s. Areas 1-3: mode general metal, 20/20/20s. Areas 4-6: mode precious metal, credit MiCorr_HE-Arc CR, C.Degrigny.

Fig. 11: X-ray tomography by cross section of the crown shows a dense and non-porous metal core (blue arrows). The corrosion products however are porous (red arrows). The external limit is visible as a fine line preserved under corrosion layers,



Credit Empa, M.Plamondon

Fig. 12: X-ray tomography by cross section of the lower part showing that there are losses of the original surface (red square),



Credit Empa, M.Plamondon.

Microstructure	Dendritic structure
First metal element	Cu
Other metal elements	Sn, Sb, Pb

Corrosion layers

The corrosion crust covers the whole object and is heterogenous. It is formed by multiple layers which are particularly hard and can hardly be removed with scalpel. The corrosion can be divided into three main layers: an outer green layer followed by a dense and hard red layer, followed by a black layer that contains corresponding markers and the limit of the original surface. In some areas this sequence is regular and clear. In other areas the limit has been replaced by more porous green-red corrosion products that do not contain any corresponding markers. In certain areas the limit and internal corrosion layers have been replaced by structural voids. XRD analysis (Table 2) of these different layers indicates that the upper hard and thick, green corrosion product (Figs. 13-14, CP1.1 and 1.2 in Figs. 6-7) is composed of copper oxychlorides: atacamite and paratacamite ($\text{Cu}_2\text{Cl}(\text{OH})_3$) (Fig. 21). The next layer (CP2) is more powdery and light green in colour (Figs. 15-16). XRD analysis also identified this product as atacamite and paratacamite (Fig. 22). During the removal of the green and red corrosion layers we found a white and waxy corrosion product close to the original surface. This observation and the presence of high amounts of copper oxychlorides led us to identify this white corrosion product as nantokite (CuCl). The localized light blue corrosion product (CP6 in Fig. 8, CP1 in Fig. 10) presents in one area on the back (Figs. 17-18) was identified as chalconatronite ($\text{Na}_2\text{Cu}(\text{CO}_3)_2 \cdot 3\text{H}_2\text{O}$) (Fig. 23). The red corrosion layer (CP3) below the copper oxychlorides and above the dark black original surface (Figs. 19-20) was identified as a mixture of cuprite (Cu_2O) as major compound

and tenorite (CuO) as minor compound (Fig. 24). It is possible that the tenorite was a contamination from the black surface below the cuprite layer.

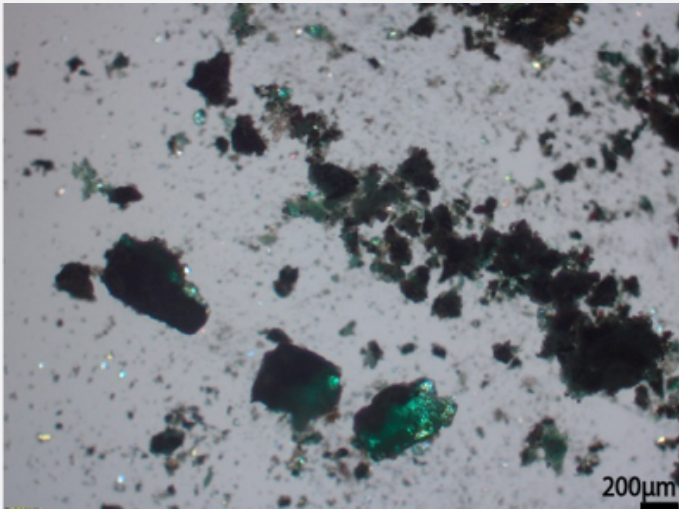
Strata	Components
CP1.1 and CP1.2	Paratacamite, Atacamite ($\text{Cu}_2\text{Cl}(\text{OH})_3$)
CP2	Paratacamite, Atacamite ($\text{Cu}_2\text{Cl}(\text{OH})_3$)
CP4	Cuprite (Cu_2O), Tenorite (CuO)
CP6	Chalconatronite ($\text{Na}_2\text{Cu}(\text{CO}_3)_2 \cdot 3\text{H}_2\text{O}$)

Table 2: Chemical composition of the corrosion products. Analytical method: XRD, credit MiCorr_Empa, A.Neels.



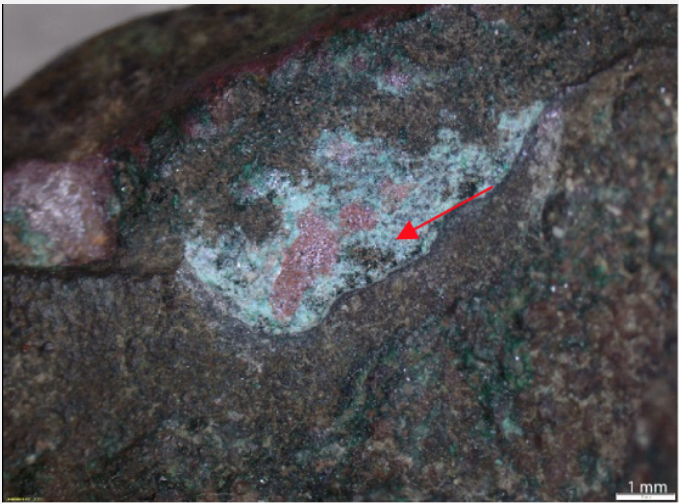
Credit HE-Arc CR, L.Pedersen.

Fig. 13: Observation of the dark green corrosion product,



Credit HE-Arc CR, L.Pedersen.

Fig. 14: Dark green corrosion product identified as paratacamite, atacamite $\text{Cu}_2\text{Cl}(\text{OH})_3$ by XRD. Microscopic examination under polarized light,



Credit HE-Arc CR, L.Pedersen.

Fig. 15: Observation of the light green corrosion product,

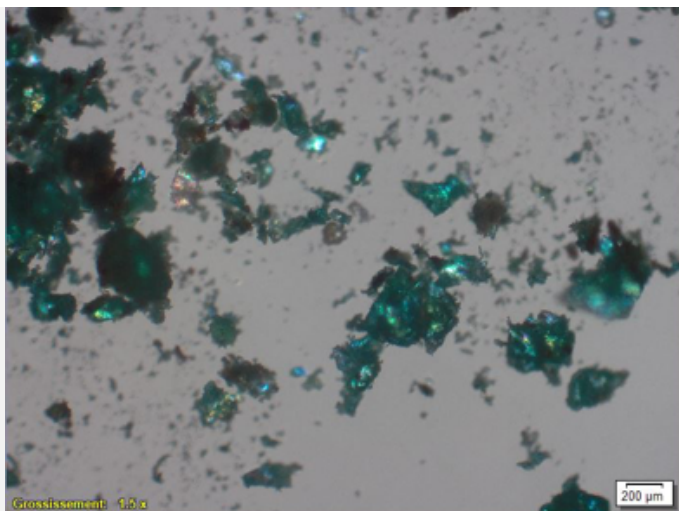


Fig. 16: Light green corrosion product identified as paratacamite, atacamite ($\text{Cu}_2\text{Cl}(\text{OH})_3$) by XRD. Microscopic examination under polarized light,

Credit HE-Arc CR, L.Pedersen.



Fig. 17: Observation of the light blue corrosion product,

Credit HE-Arc CR, L.Pedersen.

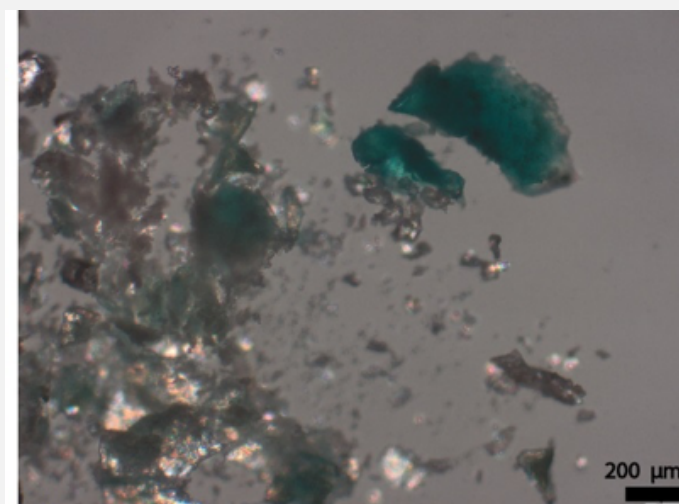


Fig. 18: Light blue corrosion product identified as chalconatronite $\text{Na}_2\text{Cu}(\text{CO}_3)_2 \cdot 3\text{H}_2\text{O}$ by XRD. Microscopic examination under polarized light,

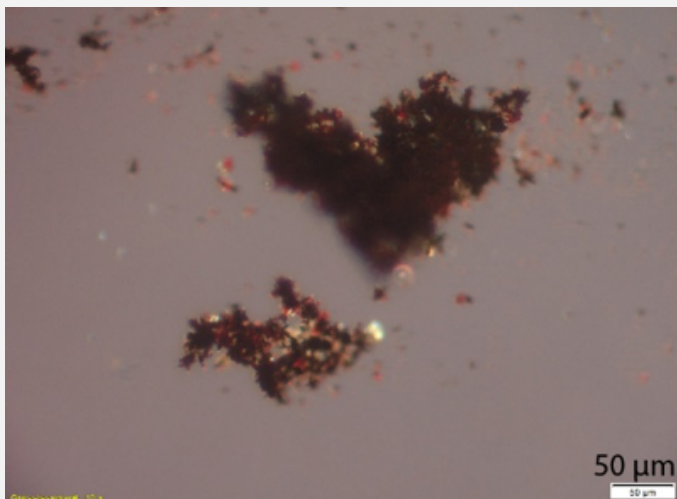
Credit HE-Arc CR, L.Pedersen.

Fig. 19: Observation of the red corrosion product above the black original surface containing corresponding markers such as engravings,



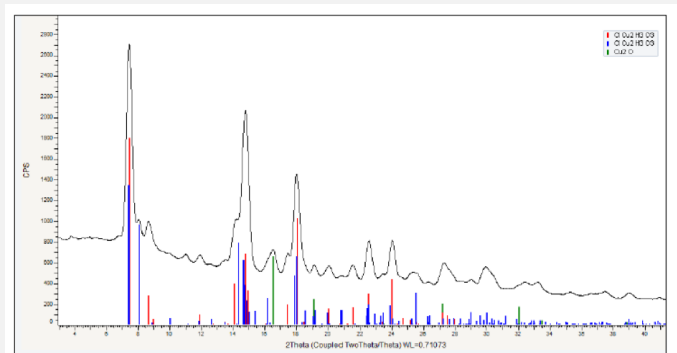
Credit HE-Arc CR, L.Pedersen.

Fig. 20: Dark red corrosion product identified as cuprite Cu_2O as major component and tenorite CuO as minor component. Microscopic examination under polarized light,



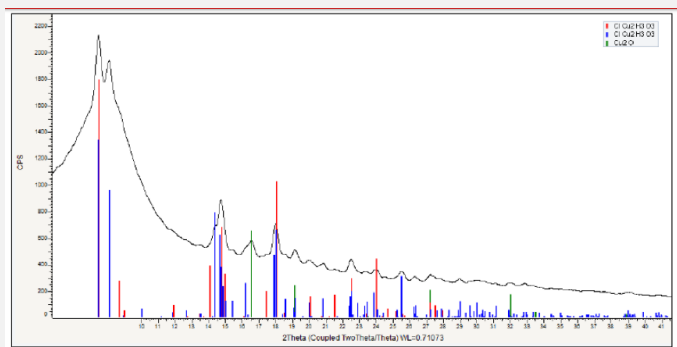
Credit HE-Arc CR, L.Pedersen.

Fig. 22: XRD spectrum of the sample from the light green corrosion product showing the presence of atacamite and paratacamite ($\text{Cu}_2\text{Cl}(\text{OH})_3$) as major compound and cuprite (Cu_2O) as minor compound,



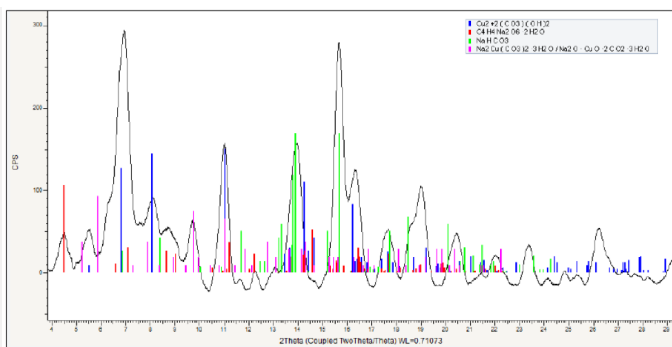
Credit Empa, A.Neels.

Fig. 21: XRD spectrum of the sample of the dark green corrosion product showing the presence of atacamite and paratacamite ($\text{Cu}_2\text{Cl}(\text{OH})_3$) as major compound and cuprite (Cu_2O) as minor compound,



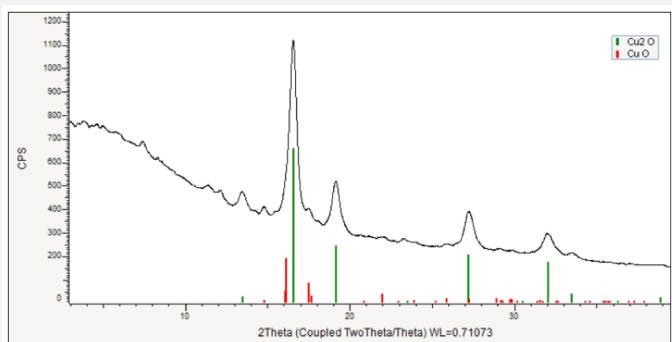
Credit Empa, A.Neels.

Fig. 23: XRD spectrum of the sample from the light blue corrosion product showing the presence of chalconatronite ($\text{Na}_2\text{Cu}(\text{CO}_3)_2 \cdot 3\text{H}_2\text{O}$). The other compounds are analysis supposition, but are not relevant,



Credit Empa, A.Neels.

Fig. 24: XRD spectrum of the sample from the dark red corrosion product showing the presence of cuprite (Cu_2O) as major compound and tenorite (CuO) as minor compound,



Credit Empa, A.Neels.

Corrosion form	Multiform
Corrosion type	Type II (Robbiola)

✎ MiCorr stratigraphy(ies) – CS

✎ Synthesis of the binocular / cross-section examination of the corrosion structure

The corrosion layers are thick and very hard due to the burial context which was probably rich in chlorides. From the top to the bottom of the corrosion layers, there is a large amount of dark and light green corrosion product identified as copper oxychlorides followed by a layer of red corrosion product identified as copper oxide (cuprite) and a dark red corrosion layer identified as copper oxide (tenorite). In certain localised areas we were able to identify chalconatronite, a light blue corrosion product typically formed by natron salt from the Egyptian soil. Due to the presence of manufacturing traces and engravings, the limit of the original surface is localised mainly in the dark red corrosion layer. In certain areas there are remains of gilding-foil identified as gold by XRF elemental analysis. The foil is preserved on the top of the corrosion layer. Because gold is a noble metal, it had not corroded and was lifted by the corrosion products of the copper alloy. Thus, the limit of the original surface is displaced in some areas (Fig. 6, see limitos).

✎ Conclusion

Thanks to the observation of the broken edge and the tomography we are able to determine that the remaining metal is well preserved. The alloy was identified by XRF as a leaded copper alloy.

The corrosion stratigraphy and the presence of a large amount of dark and light green powdery corrosion product identified as copper chlorides indicate a Robbiola Type 2 corrosion. In some areas the limit of the original surface is

well preserved and reveals a highly decorated surface. In other areas the latter did not survive and was replaced by structural voids or porous red-green corrosion products. The nature of the different corrosion products and the metal, match with what was found in other studies of Egyptian bronzes (Scott and Swartz, 2002; Gouda et al., 2012). Concerning the presence of tenorite on the original surface, tenorite generally forms if the object is exposed to high temperature or if it was intentionally heated to patinate the surface. In ancient Egyptian, heat was typically used to obtain black bronze. Tenorite is known as a corrosion product on other Egyptian black bronzes (Mohammed and Darweesh, 2012). It is likely that the Aegis has been artificially patinated. The fact that it was most certainly partly gilded reinforces this hypothesis to reach colour contrasts.

References

References object

Scott et Swartz, 2002: Scott, David et Swartz Dodd, Lynn. "Examination, conservation and analysis of a gilded Egyptian Osiris". *Journal of Cultural Heritage*, 3, 2002, p.333-345.

Gouda et al., 2012: Gouda, V.K. et al. "Characterization of Egyptian bronze archaeological artifacts". *Surf. Interface Anal.*, 44, 2012, p.1338-1345.

Mohammed et Darweesh, 2012: Mohammed, W. et Darweesh.S. "Ancient Egyptian Black-Patinated Copper alloys". *Archaeometry*, 54, 2012, p.175-192.